Experimental and model analysis of the co-oxidative behavior of syngas feed in an Intermediate Temperature Solid Oxide Fuel Cell

Elsevier Editorial System(tm) for Journal of Power Sources
Manuscript Draft

Manuscript Number:

Title: Experimental and model analysis of the co-oxidative behavior of syngas feed in an IT-SOFC

Article Type: Research Paper

Keywords: IT-SOFC; ceria; kinetics; EIS; syngas; co-oxidation.

Corresponding Author: Dr. Alessandro Donazzi,

Corresponding Author's Institution: Politecnico di Milano

First Author: Alessandro Donazzi

Order of Authors: Alessandro Donazzi; Morteza Rahmanipour; Matteo Maestri; Gianpiero Groppi; Luca Bardini; Alfonsina Pappacena; Marta Boaro

Manuscript Region of Origin: ITALY

Abstract: By means of model analysis, we show that, in the presence of syngas, the electro-oxidation of H2 and that of CO occur in parallel and contemporarily on Samaria-doped Ceria (SDC) Intermediate Temperature Solid Oxide Fuel Cells (IT-SOFCs). The activation of a co-oxidative route is a most distinguishing feature of Ce-based cells, compared to traditional SOFCs. SDC electrolyte supported IT-SOFCs with Cu-Pd-CZ80 composite anodes and LSCF cathodes were tested under a wide range of operating conditions. Polarization and EIS measurements were collected at 600°C and 650°C with syngas mixtures (between 2.3 to 0.4 H2/CO ratio), H2/N2 mixtures (from 97 to 30% H2 v/v) and CO/CO2 mixtures (from 97 to 50% CO v/v). A 1D, dynamic and heterogeneous model of the cell was applied to analyze the polarization and the EIS curves. The kinetics of the reactions of H2 electro-oxidation, CO electro-oxidation and O2 reduction were individually investigated and global power law rates were derived. The syngas experiments were simulated on a fully predictive basis and no parameter adjustment, confirming that the polarization behavior could be best reproduced exclusively by assuming the presence of the co-oxidative route. The IT-SOFCs were also exposed to biogas mixtures, revealing that the dry-reforming reaction was active.

Milan, August 7th 2015

Dear Editor of the *Journal of Power Sources*,

Please find attached our manuscript, entitled "Experimental and model analysis of the co-oxidative behavior of syngas feed in an IT-SOFC" by Alessandro Donazzi, Morteza Rahmanipour, Matteo Maestri, Gianpiero Groppi, Luca Bardini, Alfonsina Pappacena and Marta Boaro, which we would like to submit for publication.

In this paper, we present experimental and modeling results concerning the activation of a co-oxidative reaction mechanism in IT-SOFCs exposed to syngas mixtures. Novel, Ni-free, Ce-based IT-SOFCs are tested in a wide range of operative conditions, including biogas, syngas, H_2/N_2 and CO/CO_2 mixtures. By means of model analysis, we show that the electro-oxidation of H_2 and the electro-oxidation of CO are active in parallel when syngas is fed to the cell, that is, the cell is able to directly oxidize CO in addition to H_2. This is a most significant and promising result, associated to the presence of Ce in the anode formulation. For the first time in the case of IT-SOFCs, the co-oxidative mechanism is numerically demonstrated. To accomplish this task, a one-dimensional, dynamic and heterogeneous model is presented, which allows to predict both the polarization curves and the impedance spectroscopy curves. The model is based on fundamental conservation equations and also accounts for the presence of parasitic leakage currents, which characterize the behavior Ce electrolytes. A kinetic analysis is performed and power law rates are extracted for the electrocatalytic processes that are active in the cell.

The work has not been previously submitted to the Journal of Power Sources, it has not been published previously in any form and is not under consideration for publication elsewhere. All the authors and the host authorities approve the manuscript.

Thank you for your kind consideration.

Best regards,

Alessandro Donazzi

Dipartimento di Energia
Politecnico di Milano
Via Lambruschini 4
20156 Milano
e-mail: alessandro.donazzi@polimi.it

Graphical Abstract

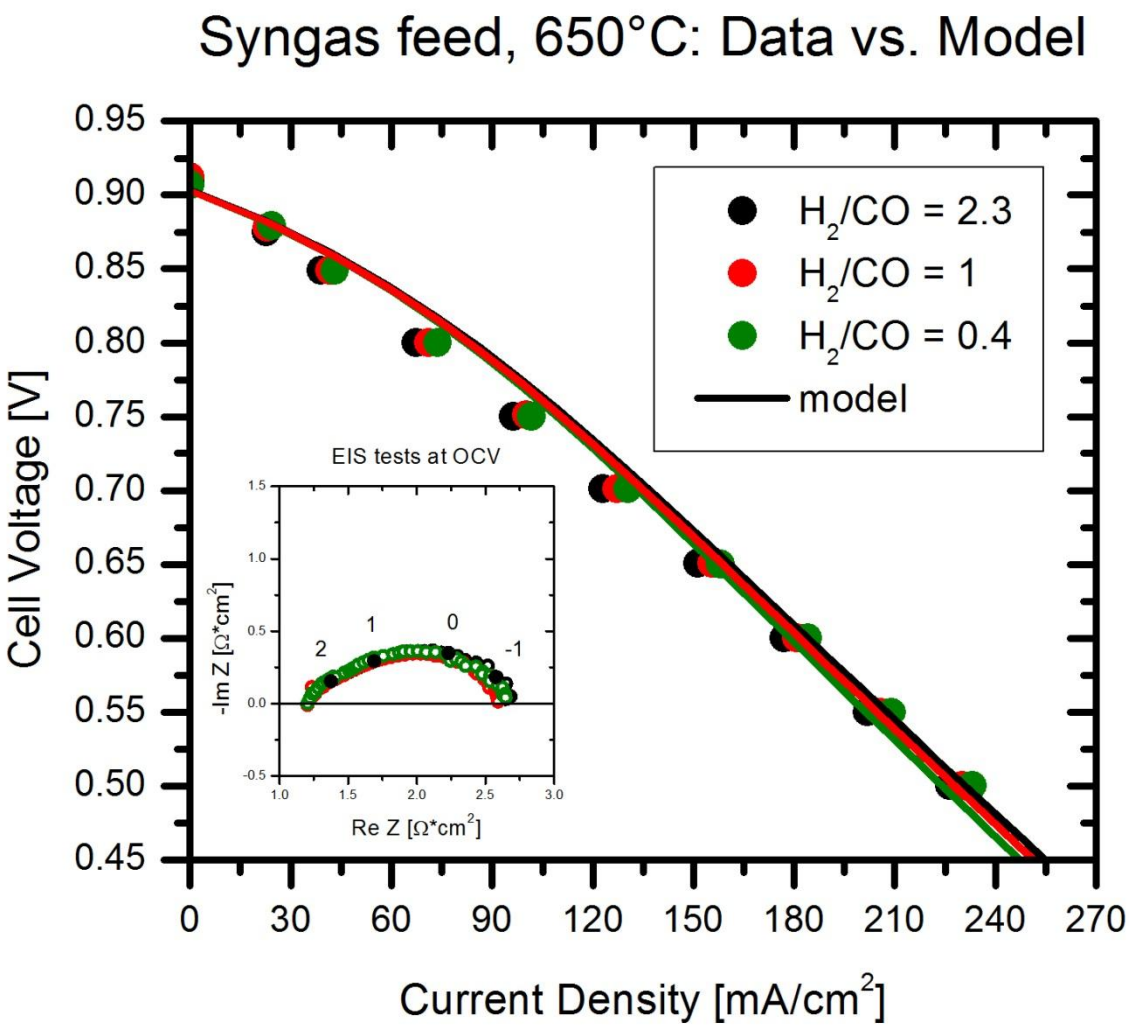

Highlights

- Ni-free, Ce-based IT-SOFCs are tested with syngas and biogas at 600 and 650°C
- The electro-oxidations of CO and of H_2 are active in parallel and contemporarily
- A 1D, dynamic, heterogeneous and physically-sound MEA model of the cell is applied
- The polarization curves and the EIS spectra are simulated based with the model
- Power law rate equations are derived for the electro-oxidation of H_2 and of CO

Experimental and model analysis of the co-oxidative behavior of syngas feed in an IT-SOFC

A. Donazzi[a*], *M. Rahmanipour*[a], *M. Maestri*[a], *G. Groppi*[a],

L. Bardini[b], *A. Pappacena*[b], *M. Boaro*[b]

[a] Dipartimento di Energia, Politecnico di Milano,

Via Lambruschini 4, 20156 Milano Italy

[b] Dipartimento di Chimica Fisica e Ambiente, Università degli Studi di Udine,

Via Cotonificio 108, 33100 Udine, Italy

*corresponding author:

Alessandro Donazzi

Dipartimento di Energia

Via Lambruschini 4, 20156 Milano (Italy)

Phone: 0039 02 2399 8651

Fax: 0039 02 2399 3318

e-mail: alessandro.donazzi@polimi.it

Abstract

By means of model analysis, we show that, in the presence of syngas, the electro-oxidation of H_2 and that of CO occur in parallel and contemporarily on Samaria-doped Ceria (SDC) Intermediate Temperature Solid Oxide Fuel Cells (IT-SOFCs). The activation of a co-oxidative route is a most distinguishing feature of Ce-based cells, compared to traditional SOFCs. SDC electrolyte supported IT-SOFCs with Cu-Pd-CZ80 composite anodes and LSCF cathodes were tested under a wide range of operating conditions. Polarization and EIS measurements were collected at 600°C and 650°C with syngas mixtures (between 2.3 to 0.4 H_2/CO ratio), H_2/N_2 mixtures (from 97 to 30% H_2 v/v) and CO/CO_2 mixtures (from 97 to 50% CO v/v). A 1D, dynamic and heterogeneous model of the cell was applied to analyze the polarization and the EIS curves. The kinetics of the reactions of H_2 electro-oxidation, CO electro-oxidation and O_2 reduction were individually investigated and global power law rates were derived. The syngas experiments were simulated on a fully predictive basis and no parameter adjustment, confirming that the polarization behavior could be best reproduced exclusively by assuming the presence of the co-oxidative route. The IT-SOFCs were also exposed to biogas mixtures, revealing that the dry-reforming reaction was active.

Keywords: IT-SOFC; ceria; kinetics; EIS; syngas; co-oxidation.

1. Introduction

Fuel flexibility is one of the most important advantages of Solid Oxide Fuel Cells compared to other types of fuel cells. In order to reduce the device volume and to intensify the power density, applications based on SOFCs for the distributed production of energy require the cell to operate with both traditional hydrocarbon fuels (CH_4 and LPG) and biomass derived fuels (biogas, ethanol). Several benefits in terms of cell lifetime and thermo-mechanical resistance are achieved by decreasing the operating temperature to 500 – 700°C, leading to Intermediate Temperature SOFCs (IT-SOFCs) [1]. Lower temperatures ask for electrolytes different from YSZ, such as Samaria-doped Ceria (SDC) and Gadolinia-doped Ceria (GDC). The adoption of these electrolytes activates an internal short circuit current due to the partial reduction of the Ce^{4+}/Ce^{3+} couple, which lowers the cell performance and asks for the introduction of insulating barriers (e.g. ScSZ) in case of applicative purposes [2, 3]. Novel materials are also required for the anode and the cathode, due to compatibility issues (formation of secondary phases, interdiffusion, delamination) and thanks to the possibility of optimizing the composition in order to increase the low temperature activity. Along with this, double-layered perovskite oxides are state of the art cathodes for IT-SOFCs [4]. With reference to the anode, Cu-based and Ce-based compounds have been widely explored in the literature. The addition of Cu is known to strongly inhibit the production of coke, even in the presence of dry methane feed, and to provide the necessary electronic conductivity to the electrode [5, 6]. Ceria is exploited for its oxygen ion transfer capability, which makes it a very effective oxidation catalyst and allows to increase the volume active for the electro-oxidation, deepening the penetration distance of the C-removing oxygen ions and keeping the surface clean from coke [7]. Addition of noble metals (Pd, Rh or Pt) at dopant levels

has been proved to boost the activity of Ce-based anodes, especially in the presence of methane and biogas, thanks to the increase in the reforming chemistry [8, 9].

The adoption of novel composite materials triggers different catalytic and electrocatalytic routes compared to traditional Ni-based anodes, especially those processes related to the conversion of syngas and hydrocarbons. In light of this, it is generally understood that negligible direct electro-oxidation occurs when light hydrocarbons are supplied to the cell. Instead, the fuel is primarily reformed or partially oxidized to H_2 and CO rich mixtures (syngas). A question of interest is how H_2 and CO undergo the electro-oxidation process when they are mixed together in the anode: whether or not the oxidation of H_2 prevails on that of CO, or if a co-oxidation pathway is feasible. Additionally, the oxidation of syngas leads to the production of CO_2 and H_2O, whose counter diffusion further enhances the steam reforming and the dry reforming catalytic chemistry, as well as the Water Gas Shift (WGS) equilibrium. These heterogeneous processes can possibly contribute to the balance between the electro-oxidation of H_2 and CO. Several efforts have therefore been devoted to unravel the mechanism of the electro-oxidative processes, in order to optimize the electrode design. In a comprehensive review, Gohniem and coworkers [10] have recently addressed the chemistry of the electro-oxidation of H_2 and CO, both individually and in the case of syngas mixtures: in Ni-YSZ anodes, the electrochemical conversion of syngas is governed by the H_2 electro-oxidation, with the WGS reaction being responsible for the conversion of CO to H_2O and H_2, for further electrochemical consumption. H_2 is the dominant electroactive species, whereas CO is not directly electro-oxidized: since the electro-oxidation kinetics of H_2 are much faster than the electro-oxidation kinetics of CO (up to one order of magnitude), H_2 remains the favored electroactive species even when the excess of CO is significant [11]. Ultimately, the reason for this lies in the spillover and surface

diffusion rates of H, which are much faster than those of CO, and allow for an easier transfer of H from the Ni metal site to the YSZ surface (where O^{2-} ions are provided). Much less investigation on this subject is reported for Ce-based anodes. Notably, however, when using Cu-CeO_2-YSZ anodes in the presence of syngas mixtures, Costa-Nunes et al. [12] found that Ceria was active for both the electrochemical oxidation of H_2 and CO, contemporarily. That is, no predominance of the H_2 electro-oxidation was found, differently from Ni-YSZ anodes: possibly, this behavior could be attributed to the specific roles of Ceria and Cu, wherein the metal is almost inert and the spillover and diffusion reactions are blocked, while Ceria is active in both the oxidation of H_2 and CO.

Given the possibility of novel mechanistic routes, the research of materials must be closely accompanied by numerical model analysis to rationalize the chemical and physical phenomena occurring in the cell. Several electrochemical models are present in the literature, with different degrees of complexity with respect to both the approach and the kinetic schemes. Schemes ranging from detailed microkinetic mechanisms for the heterogeneous chemistry and the charge transfer chemistry [13-17] to Butler-Volmer frames with global power law rates [18, 19] have been successfully applied. As well, different approaches have been validated, spanning from particle-level descriptions of the electrode microstructure [20, 21] to mean-field descriptions that take into account average morphological parameters and average material properties [22]. Most of this models are devoted to traditional cells: in the case of novel material formulations, due to the lack of kinetic data and to the complexity of the electrodic compositions, physically-based membrane-electrode-assembly (MEA) models using global kinetic rates are well fitted and sufficiently informative.

In the present work, we show that the oxidation of CO and the oxidation of H_2 occur in parallel, and not in a mutual exclusive way, when syngas is fed to a Ce-based IT-SOFC. SDC electrolyte-supported IT-SOFCs with Cu-Pd-CZ80 composite anodes and LSCF cathodes were tested in the presence of syngas and biogas mixtures. Polarization and impedance measurements were carried out at 600 and 650°C, over a wide range of gas compositions. A 1D, dynamic and heterogeneous model of the IT-SOFC, accounting for the presence of internal shorting currents and for the WGS chemistry, was applied to rationalize the behavior observed with syngas. The kinetics of the H_2 electro-oxidation and of the CO electro-oxidation were individually investigated with dedicated H_2/N_2 tests and CO/CO_2 tests. Power law kinetic equations were derived, which allowed to simulate the cell behavior in the presence of syngas. The comparison between model simulations and experimental measurements revealed that the best description could be achieved exclusively by assuming the presence of the co-oxidative route.

2. Experimental and theoretical tools

2.1 Materials and experimental methods

Electrolyte supported button cells (20 mm diameter, 0.82 cm^2 cathode area) were prepared and tested. The morphological properties of the cells are summarized in Table 1. 20 wt% Samarium doped Ceria ($Sm_{0.2}Ce_{0.8}O_{1.9}$, SDC) was chosen for the electrolyte and for the porous scaffold of the anode. To form the electrolyte and the scaffold, SDC powders containing starch (30 wt%) as pore former were uniaxially pressed with pure SDC powders. This bilayer was calcined in air at 1400°C for 3 h, producing a porous 150 μm thick SDC scaffold supported on a dense 380 μm thick SDC electrolyte. After forming the anode and the electrolyte, the LSCF cathode (40

μm) was brushed on the opposite side of the cell and calcined at 1250°C for 3 h to reach adhesion. The anode was prepared via the infiltration technique [23]. The porous SDC scaffold was first impregnated with a nitric solution Pd and CZ80 (20 wt% CeO_2, 80 wt% ZrO_2, 1 wt% Pd in the Pd/CZ80 solution) and then calcined at 600°C. The steps of impregnation and calcination were repeated until the desired amounts were loaded. Once the Pd and CZ80 components were loaded, the nitric solution containing Cu was added to the scaffold and the steps of impregnation and calcination were repeated. The final anode composition was 15 wt% Cu, 0.15 wt% Pd and 15 wt% CZ80. The complete cell was calcined at 700°C for 3 h. Wet impregnation with water was applied to estimate the porosity of the electrodes, which amounted to 40% in both cases. After testing, the morphological features of the cells were assessed via Scanning Electron Microscopy (SEM) using a Carl Zeiss EVO50VP instrument equipped with an Energy Dispersive Spectrometer (EDS) for elemental analysis. The post-mortem analysis of the electrodes (Fig. 1) revealed no interdiffusion of the elements (the Ce peaks in the cathode side were residuals of the mechanical breakage) and no discontinuity in the electrolyte/electrode interfaces. The continuity among the particles and the contact between the electrodes and the electrolyte were both good.

Polarization and EIS experiments were carried out between 600 and 700°C with 100 Ncc/min air flow and 30 Ncc/min anodic flow, under constant humidification (3% H_2O at room temperature). Silver meshes and ink were applied to collect the current on both the electrodes. A potentiostat/galvanostat (Amel 7050) equipped with a frequency response analyzer (520 FRA, Materials Mates) was used for the measurements. The experiments were performed with:

- syngas mixtures at varying the H_2 to CO ratio between 2.3 to 0.4, from 70% to 30% H_2 v/v with CO to balance (dry basis);

- H_2/N_2 mixtures at varying the partial pressure of H_2 from 100% to 30% v/v (dry basis);
- CO/CO_2 mixtures at varying the partial pressure of CO from 97% to 50% v/v with CO_2 to balance (dry basis).

Experiments were also carried out with biogas (CH_4/CO_2 75:25 v/v). The polarization measurements were performed by ramping the voltage from the OCV value (Open Cell Voltage) down to 0.5 V with 50 mV steps. Voltage values lower than 0.5 V were never reached, to avoid the re-oxidation of the anode metal elements and the subsequent instability of the cell. The EIS experiments were performed at the OCV, with 50 mV voltage amplitude and between 10 mHz and 1 kHz. The EIS curves were always collected prior to the polarization experiments.

2.2 SOFC model

The experimental results were analyzed with a one dimensional, heterogeneous, dynamic and isothermal model of the button cell. The model allows to predict the cell voltage as a function of the current density, the temperature, the pressure and the feed composition. Both polarization curves and impedance spectra were simulated. The model equations and the boundary conditions are reported in Table 2. The model rigorously describes the reaction with diffusion problem by coupling the mass balance equations (Eq. 1) with the equations of the Dusty Gas Model (Eq. 2) for the diffusion of the species within the porous matrix of the electrodes. Both molecular and Knudsen diffusion processes are taken into account. The cell voltage is estimated by subtracting from the Nernst potential all the contributions of the different losses, that is, the activation losses due to the electrochemical reactions in the electrodes and the ohmic resistance (Eq. 4). Given

that the Nernst potential is estimated at the interface between the electrode and the electrolyte (P^{W}_{i} in the equations), the concentration losses are already accounted for and need not to be declared in the equation. The activation losses are calculated according to the Butler-Volmer formalism (Eq. 5 and 6). Due to the use of SDC, an internal short-circuit current was present in the electrolyte, which decreased the total current extracted from the cell and affected the value of the OCV [3, 24]. The scheme first proposed by Riess in Ref. [25] and later included in a model for complete SOFCs by Leah et al. [26] was applied in the calculation. At each voltage, the total current extracted from the cell (i_{total} in Eq. 8) results from the difference between the current density associated with the flow of oxygen ions through the electrodes and the electrolyte (i_{O2-}), which is responsible for the polarization losses, and the leakage current due to the internal short-circuit ($i_{leakage}$). The equation derived by Sahibzada et al. [27] (Eq. 9) is applied to estimate the leakage current density. It is worthy to note that the leakage current is a function of the ionic current density and of the cell voltage, as well as of the ionic conductivity and of the electronic conductivity of the electrolyte (Eq. 17 and 18, Table 3). In the equation for $i_{leakage}$, the term referred as P^{θ} is defined as the value of the oxygen partial pressure P^{W}_{O2} at which the ionic and electronic conductivities of the electrolyte become equal.

With respect to the boundary conditions (Eq. 10 – 13), the CSTR equations were chosen at the gas/electrode interface, which were expressed via the continuity of molar flows. This choice is in line with the absence of radial gradients of composition along the electrodes surfaces, due to the high flow rates of the feed gas and to the small dimensions of the cell. Since the electrochemical charge transfer reactions were assumed to take place exclusively in the triple-phase boundary (TPB) region located at the electrode/electrolyte interface, the boundary condition was set as the equality

between the current density and the diffusive molar flow rates, according to the stoichiometric coefficients of the electrochemical reaction (Eq. 13).

With respect to the kinetics, the reaction scheme considered in the model includes the electrochemical oxidation of H_2 and the electrochemical oxidation of CO at the anode/electrolyte interface, the reduction of O_2 at the cathode/electrolyte interface, and the Water Gas Shift reaction in the anode porous matrix. Global, power law rate equations (Table 3) were used to describe the equilibrium exchange current densities of the charge transfer reactions (Eq. 14 – 16).

The model was also applied to simulate the measured impedance spectra. The corresponding equations are reported in Table 4. An alternate current is imposed to the cell (Eq. 19) by assigning the mean value ($i_{Average}$), the perturbation amplitude (i_P) and the frequency (ω). As a result, when the perturbation amplitude is sufficiently small, a stable harmonic cell voltage is achieved, usually after 15 periods. At each value of the frequency, the impedance Z (Eq. 21) stems from the ratio of the alternate voltage and the alternate current. Specifically, the voltage perturbation amplitude E_P and the phase lag φ are calculated via integration of the cell voltage over the last two periods t_P:

$$E_P \cdot \cos(\varphi) = \frac{2}{t_P} \cdot \int_0^{t_P} E_{Cell}(t) \cdot \sin(\omega t) \cdot dt \qquad (26)$$

$$E_P \cdot \sin(\varphi) = \frac{2}{t_P} \cdot \int_0^{t_P} E_{Cell}(t) \cdot \cos(\omega t) \cdot dt \qquad (27)$$

The impedance values Z calculated in Eq. 21 do not allow for a full description of the different arcs of the EIS spectrum: indeed, due to the absence of the charge balances in the system of equations (i.e. due to exclusion of fundamental equations for double layer charging phenomena), the activation resistances associated

to the charge transfer reactions (R_{Act}^{An} and R_{Act}^{Cat}) can not appear as arcs in a Nyquist plot, and their value is included only in the limit of Z at high frequency ($\omega \rightarrow +\infty$). For this reason, to derive the complete impedance spectrum and to restore its physically sound appearance, the approach proposed by Zhu and Kee [28] was adopted. In this approach, the impedance curve is derived based on an equivalent circuit representation. In the circuit, the activation resistances are considered in parallel with double layer capacitances (C_{DL}^{An} and C_{DL}^{Cat}); in turn, these two elements are put in series with the ohmic resistance and with the diffusive resistance Z_{Diff}, which is a resistance term due to the gas diffusion and to the heterogeneous chemistry occurring in the anode volume. Aside of the contribution related to the internal gas diffusion, the gas conversion impedance [29] is also taken into account in the Z_{Diff} term, thanks to the presence of the CSTR condition at the boundary layer. Following the approach outlined in [28], the activation resistances are calculated according to Eq. 22 and 23. The diffusive resistance Z_{Diff} is then calculated by subtracting the ohmic resistance and the activation resistances from the impedance Z (Eq. 24). The final impedance, herein referred to as total impedance Z_{Total}, is given by Equation 25, wherein the terms related to the RC elements resulting from the parallel between the double layer capacity and the resistance can be easily individuated.

2.3 Equations for the oxidation of syngas

In SOFC modeling, it is generally assumed that only one fuel species is electro-oxidized at the anode side. Differently, in the present work, the activation of a co-oxidative process was assumed for the analysis of the tests with syngas. In the calculations, the approach suggested by Iwai et al. [30] was adopted. In this approach, the electro-oxidation of H_2 ($H_2 + O^{2-} \rightarrow H_2O + 2e^-$) and that of CO ($CO + O^{2-} \rightarrow CO_2$

+ $2e^-$) are treated as an electrical parallel, meaning that the total current flowing through the cathode (i_{O2-}) is split in two current contributions at the anode, one due to H_2 (i_{H2}) and the other due to CO (i_{CO}):

$$i_{O^{2-}} = i_{H_2} + i_{CO} \qquad (28)$$

In each branch of the parallel, the theoretical Nernst potential of the anodic semi-reaction is considered in series with the corresponding activation polarization. When current is drawn from the cell, this parallel expresses the following relation:

$$E_{Nernst}^{H_2} - \eta_{Act}^{An,H_2} = E_{Nernst}^{CO} - \eta_{Act}^{CO} \qquad (29)$$

The introduction of this assumption in the solving system was realized by substituting the cell potential equation (Eq. 4) with the following two equations:

$$E_{Cell} = E_{Nernst}^{H_2} - R_{Ohm} \cdot i_{O^{2-}} - \eta_{Act}^{An,H_2} - \eta_{Act}^{Cat} \qquad (30)$$

$$E_{Cell} = E_{Nernst}^{CO} - R_{Ohm} \cdot i_{O^{2-}} - \eta_{Act}^{An,CO} - \eta_{Act}^{Cat} \qquad (31)$$

Also the boundary conditions at the electrolyte/electrode interface were changed consistently, meaning that the stoichiometric coefficients of the semi-reactions of H_2 and CO electro-oxidation were considered in the balance between the diffusive flow rates and the current (Eq. 13). No change was instead required in the boundary condition of O_2.

2.4 Solving procedure

It is widely reported [31, 32] that the DGM equations, in their implicit form, lead to an ill-conditioned system and therefore need to be rearranged to allow for a numerical solution. A comprehensive discussion with reference to SOFC modeling is

given by Zhou et al. in [17], which is followed in the present work. The issue is overcome by writing the diffusive molar flows J_i in a Fickian explicit form:

$$J_i = -\left[\sum_{i}^{Nspecie} D_{ij}^{DGM} \cdot \nabla C_j\right] - \left[\sum_{i}^{Nspecie} D_{ij}^{DGM} \cdot \frac{C_j}{D_j^{Knu,eff}}\right] \cdot \frac{B}{\mu} \nabla P \qquad (32)$$

In the equation, the D_{ij}^{DGM} terms are calculated by inverting of the diffusive matrix H ($[D^{DGM}] = [H]^{-1}$), whose terms are defined by:

$$H_{ij} = \left[\frac{1}{D_j^{Knu,eff}} + \sum_{i \neq j}^{Nspecie} \frac{C_j}{D_{ij}^{Mol,eff}}\right] \cdot \delta_{ij} + \frac{C_j}{D_{ij}^{Mol,eff}} \cdot \left(\delta_{ij} - 1\right) \qquad (33)$$

In the numerical procedure, the equations of the DGM were thus written in the form given in Eq. (32).

The model consisted of 12 partial differential equations coupled with 8 algebraic equations, and was solved numerically by the method of lines [33]. The axial electrodes length was split into a suitable number of grid points. In each point, the spatial derivatives were approximated by the Euler backward differentiation method. The DAE system was solved by the initial value LSODI routine for stiff problems in Fortran environment. The convergence of the solution was verified by varying the number of grid points along z (30 points were adequate). The dynamic problem for the calculation of the impedance Z was solved starting from the steady state solution, calculated at the mean current density value. A perturbation amplitude equal to 1 $\mu A/cm^2$ was always used, which guaranteed a linear response of the cell voltage. In the time domain, the dynamic system was integrated for 20 periods, and only the last two were used for the calculation of the impedance. Once the oscillating response was obtained, the procedure reported in Table 4 was applied to derive the Nyquist plot and the Bode plots.

3. Results

3.1 Experiments with syngas mixtures

The cell was exposed to syngas mixtures at varying the H_2 to CO ratio from 2.3 to 0.4, under constant humidification. The polarization curves and the impedance spectra were collected at 600°C and 650°C, upon decreasing the partial pressure of H_2 from 70% v/v to 30% v/v (dry basis) and maintaining the CO fraction to balance. The results are reported in Figure 2: in the plots with the polarization curves (panels a and b), the continuous lines refer to the model simulations and are discussed in the dedicated section. With respect to the polarization curves, it is immediately noted that almost no variation was found passing from a ratio of 2.3 to a ratio of 0.4: at both the temperature levels, the OCV values maintained constant, so as the slope and the current extracted at 0.5 V. The same effect was well appreciated in the EIS spectra collected at the OCV (panels c and d): no significant variation was found and the arcs almost entirely overlapped over the whole operating range, maintaining constant polarization resistances of 1.45 $\Omega*cm^2$ at 650°C and 3 $\Omega*cm^2$ at 600°C. These results are significant: one the one hand, they suggest that, in the presence of syngas, both the H_2 electro-oxidation and the CO electro-oxidation were occurring in parallel and contemporarily; one the other hand, the capability of activating a co-oxidative route for CO and H_2 could be in principle a unique feature of Ce-based anodes. Indeed, in the case of Ni-YSZ SOFCs [10], it is generally understood that the cell either behaves exclusively as a H_2 oxidizer, or it behaves exclusively as a CO oxidizer: in the first case, at decreasing the H_2 pressure, a decrease of the extracted current would be observed at constant voltage, a case which was not observed here when passing from 70% H_2 to 30% H_2; in the second case, upon increasing the partial pressure of CO, an

increase of the current would be observed at constant voltage, which was also not observed in the experiments with syngas when CO grew from 30% to 70%. A compensation effect therefore emerged, which was likely associated to the parallel oxidation of H_2 and CO: the hindrance expected upon lowering the H_2 concentration was supported by the promotion of CO oxidation at increasing the concentration of CO. Due to the overlapping of two different chemical routes, the one of H_2 oxidation and the one of CO oxidation, a more comprehensive insight on this co-oxidative effect was possible only based on the numerical model analysis of the polarization curves (presented in Section 4). In order to address this task, experiments were performed on H_2/N_2 mixtures and on CO/CO_2 mixtures, so that the H_2 oxidation behavior and the CO oxidation behavior could be analyzed individually and their rates estimated independently.

3.2 Experiments with H_2/N_2 mixtures

Polarization and impedance experiments with humidified H_2/N_2 mixtures were performed at 600 and 650°C. The partial pressure of H_2 was decreased from 97% v/v to 29% v/v with N_2 to balance. The polarization curves are reported in the panels a and b of Figure 3. OCV values of 0.905 V and 0.95 V were achieved at 650°C and 600°C respectively, which maintained constant upon decreasing the partial pressure of H_2 (Tab. 6). These values, lower than the Nernst potentials at the same temperature and H_2 pressure, are a consequence of the short circuit current that establishes in the SDC electrolyte due to its mixed ionic and electronic conduction. The values measured are in line with those reported in the literature for IT-SOFCs based on SDC electrolytes and running on humidified H_2: Fuerte et al. [24] show an OCV close to 0.85 V with Cu-Co-Ce/SDC/LSM cells at 600°C; Zhang et al. [34] report an OCV of

0.85 V at 650°C and an OCV of 0.875 V at 600°C, when testing Ni-SDC/SDC/SSC cells supported on a thick Ni-YSZ cermet; Liu et al. [35] find OCV values between 0.7 V and 0.9 V at 600°C when testing Ni/SDC/LSCF cells with different electrolyte thickness (200 – 800 μm). With respect to the polarization curve, the maximum current extracted in the experiments (240 mA/cm^2 with 97% H_2 at 0.5 V and 650°C) accounted for only 4% conversion of H_2, whereas, at the lowest H_2 concentration, the conversion values rose up only to 11% (Tab. 6). In both cases, a decrease of the performance was observed upon lowering the H_2 amount, that suggested a positive order in the partial pressure of H_2 for the rate of the H_2 electro-oxidation.

The results of the EIS experiments are reported in the panels c and d of Figure 3. The values of the polarization resistance (R_{Pol}) measured as a function of temperature and P_{H2} are plotted also in Figure 5b. A single depressed arc was always observed, coherently with the presence of overlapping contributions from the cathodic activation, the anodic activation and mass transfer. As expected, the polarization resistance increased upon decreasing the temperature, passing from 1.45 Ω*cm^2 at 650°C and 97% H_2 to 2.5 Ω*cm^2 at 600°C. As well, the polarization resistance increased upon decreasing the H_2 partial pressure. In this latter case, the growth of the arcs mainly occurred in the mid to low frequency range (1 Hz – 10 mHz): given that mass transport generally influences the low frequency range, the results suggest that the kinetic processes related to the anode were detected at mid frequency, and those of the cathode in the high frequency range. An inspection of the spectra also reveals that the ohmic resistance slightly increased at decreasing the H_2 partial pressure, within 0.5 Ω*cm^2 at 650°C and 0.25 Ω*cm^2 at 600°C. This effect, which was neither due to gas leakage nor to local temperature variations, had possibly a chemical cause: indeed, the electrical conductivity of SDC varies with the reducing potential, leading to a variation of the ohmic resistance. Structural causes such as local delamination are

less likely, given that the effect was reversible and the ohmic resistance was recovered upon increasing the H_2 pressure.

3.3 Experiments with CO/CO_2 mixtures

Experiments with CO/CO_2 mixtures were also carried out at 600°C and 650°C to gain kinetically valuable information on the electro-oxidation of CO. The amount of CO was decreased from 97% v/v to 50% v/v (dry basis) and the amount of CO_2 was increased to balance. Figure 4 shows the results of the polarization curves. The results of the EIS experiments performed at the OCV are reported only in form of polarization resistance in Figure 5d. As expected, a picture similar to that of the H_2 electro-oxidation was obtained, with a loss of performance at decreasing the concentration of CO, which evidenced either a positive dependence of the oxidation kinetics on CO or an inhibiting effect due to CO_2. The current extracted decreased (Fig. 4a-b) and the polarization resistance increased (Fig. 5d) with decreasing CO pressure. In line with the lower activity of the cell in the electro-oxidation of CO compared to that of H_2, the current densities extracted at 0.5 V were always lower than those measured with the H_2/N_2 mixtures (152 mA/cm^2 with 97% CO vs. 182 mA/cm^2 with 97% H_2 at 600°C) and gave rise to smaller conversions (never higher than 6.5%, Table 7). The OCV values were equal to 0.953 V at 600°C and 0.913 V at 650°C and lowered at decreasing the partial pressure of CO, differently from what observed with H_2.

The results of the EIS tests mirrored those discussed for the H_2/N_2 mixtures, although higher polarization resistances were observed, coherently with a slower activity towards CO oxidation compared to that of H_2 oxidation. Again, an effect of variation of the ohmic resistance was detected when passing from 97% to 50% CO,

with similar entity of that observed in Fig. 3c and d for H_2/N_2 mixtures. Overall, the results obtained with CO/CO_2 mixtures show that the cells was less active in the oxidation of CO than in the oxidation of H_2, in line with general literature findings [11].

3.4 Experiments with biogas

The cell was exposed to a humidified synthetic biogas mixture (75% CH_4 and 25% CO_2 on dry basis) in order to test the reforming capability. The experiments (Fig. 6a) were carried out between 600°C and 700°C. At all the temperatures, upon switching to biogas from a humidified pure H_2 mixture, the OCV dropped and reached the stability after 1 hour. Contrary to the Nernstian behavior, the OCV values grew with temperature, passing from 0.62 V at 600°C to 0.68 V at 700°C. This growth suggested that, in the presence of biogas, the cell was limited by the kinetics of the dry-reforming reaction ($CH_4 + CO_2 \rightarrow 2\ CO + 2\ H_2$), which produced H_2 and CO for the subsequent electro-oxidation processes. Indeed, as reported in the experiments with syngas, i.e. where CO and H_2 were directly supplied, the OCV decreased with temperature instead of increasing: in the case of the biogas, the increase could be justified based on the increase of the endothermic dry reforming rate. These OCV values were in line with those reported in the literature for similar cells tested in the presence of biogas [34], though still too low to meet applications. Nonetheless, it shall be noted that the cells were electrolyte-supported, with thin anodes: thicker anodes could have improved the extent of the reforming reaction, leading to higher OCVs. In order to further prove that the production of syngas was the limiting step, after 3 hours under synthetic biogas, the mixture was enriched with H_2 and CO at the expenses of CO_2 and a composition of 50% CH_4, 20% CO_2, 20% H_2

and 10% CO (dry basis) was supplied. Figure 6b shows that high values of the OCV were quickly restored, comparable with those achieved with syngas.

4. Mathematical model analysis

The most significant result of the experimental investigation is the possibility that the electro-oxidation of CO was active in parallel to the electro-oxidation of H_2 when syngas was fed to the cell, giving rise to a co-oxidative reaction pathway capable of maintaining a constant performance when the H_2/CO ratio was varied. In order to prove this effect, numerical analysis with the model was necessary. Though, a direct analysis of the syngas system was complex, since the anodic kinetics of CO oxidation possibly overlapped with the kinetics of H_2 oxidation, as well as with the cathodic O_2 reduction kinetics. Under this light, the experiments with H_2/N_2 mixtures constituted a sub-system that allowed to independently derive the rate equation of the H_2 electro-oxidation. As well, the experiments with CO/CO_2 mixtures allowed to independently derive the rate equation of the electro-oxidation of CO. Indeed, due to the low conversion and due to the fact that the voltage never approached the diffusion limited region, the experimental results were informative of the intrinsic kinetics of the process. Once the two sub-systems were characterized, the experiments with syngas mixtures could be simulated on a fully predictive basis, with no parameter adjustment. Following this approach, it is important to note that the results of the EIS experiments were used to derive the kinetic equations and the corresponding parameters. Global power-law equations were adopted (Table 3), whose parameters (pre-exponential factor of the exchange current density, reaction order of the species and activation energy) were obtained by best fitting of the curves. The parameters that allowed for the closest match between data and simulations are reported in Table 5.

Once the kinetic equations were derived, the polarization curves were used to verify the agreement between the predictions and the experimental data. The rate of H_2 oxidation and O_2 reduction were derived first, then those for the oxidation of CO. The ohmic resistance, in terms of conductivity and activation energy, was estimated based on the EIS measurement obtained with humidified H_2 mixtures (97% H_2 and 3% H_2O), without taking into account the effect of increase observed at decreasing the H_2 pressure. The values estimated for the activation energy (48.5 kJ/mol) and the pre-exponential factor ($1.39*10^4$ S*K/cm) fell within the range (43 – 62 kJ/mol and $4.5*10^3$ – $2.2*10^4$ S*K/cm) given in the literature for SDC [3, 36, 37]. The SEM pictures allowed to measure the thickness of the layers and also provided a rough estimation of the particle size (2 μm, inserts of Fig. 1). The porosity was determined via H_2O impregnation (Section 2.1), whereas values of tortuosity of 6 were assumed, which are typical in the literature [17, 28]: it shall be noted however that these latter parameters negligibly affected the simulations.

4.1 H_2 electro-oxidation

The results of the impedance tests carried out on H_2/N_2 mixtures were applied to extract the anodic H_2 oxidation kinetics. In parallel, the results of impedance tests at varying the O_2 content from 21% to 10% and 5% (Fig. 5c) were used for the cathodic kinetics. In this case, given that LSCF has been widely studied in the literature, the activation energy (139 kJ/mol) and charge transfer parameters for the Butler-Volmer equation ($\alpha^{Cat}_A = 0.65$ and $\alpha^{Cat}_C = 0.35$ with 2 electrons) were set equal to those discussed by Leonide et al. [18]. The O_2 order and pre-exponential factor k_{O2}^{Re} were estimated; the estimation of k_{O2}^{Re} is consistent with the fact that it typically includes morphological parameters, such as the extension of the TPB, which are

determined by the microstructure and therefore are expected to change with the preparation procedure. In the case of the rate of the H_2 oxidation, the charge transfer coefficients of the Butler-Volmer equation were considered equal to 0.5 with 2 exchanged electrons, while the activation energy, the pre-exponential factor k_{H2}^{Ox} and the reaction order of H_2 were adjusted. No information could be extracted regarding the order of H_2O, due to the low conversion of H_2, which did not allow for significant variations of the H_2O concentration.

The results are presented in the panels a to c of Figure 5. It is important to note that only the polarization resistance could be correctly reproduced by the model, and therefore only the real parts of the impedance spectra (R_{Pol}) were taken into account in the derivation of the kinetic rate. This is a specific limit of the approach followed in the calculation of the impedance curves, which is due to the absence of the charge balance in the solving system. Indeed, the model rigorously calculates the overall amount of the polarization resistance, but fails in following the shape of the impedance curve. An example is provided in Figure 5a with respect of the spectra obtained at decreasing the amount of H_2 at 650°C (the spectra were aligned by subtracting the ohmic resistance): it can be seen that the imaginary part of the curve, which is directly related to the double layer effects, could be reproduced only in terms of semi-circular arcs. In the simulations, a capacitance value of 50 $\mu F/cm^2$ for the cathode and a value of 500 $\mu F/cm^2$ for the anode allowed for the best approximation. In the simulations, the first arc belonged to the cathodic activation polarization; the second, larger arc was associated to the anodic activation polarization; the small arc in the low frequency zone, was due to the gas diffusive resistance outside the anode. Coherently with the small thickness of the anode, the internal diffusive resistance resulted smaller and overlapped with the anodic arc. Notwithstanding with limits in reproducing the imaginary part of the impedance, a coherent description of the

polarization resistance was obtained for both the impedance tests at varying O_2 and H_2 concentration (Fig. 5b and c). A reaction order of 0.47 was estimated for the partial pressure of H_2, i.e. close to 0.5, which suggested that the rate determining step of the H_2 oxidation kinetics was a charge transfer reaction involving a H species produced by dissociative adsorption of H_2. A reaction order of 0.33 was found for the cathode: this value is in fair agreement with the order of 0.22 estimated in [18].

The kinetic rates were applied for the simulation of the H_2/N_2 polarization curves at 600°C and 650°C (Fig. 3a and 3b). Prior to the simulation of these curves, the activation energy and the pre-exponential factor of the electronic conductivity of the SDC electrolyte were estimated based on the best fit achieved to predict the OCVs of the mixtures at 97% H_2; the values obtained (220 kJ/mol for the activation energy and $3.5*10^8$ $S*atm^{0.25}*K/cm$ for the pre-exponential factor, Table 5) were adopted for all the simulations of the work. Noteworthy, these values were in reasonable agreement with the literature, considering that their range is wide ($2.2*10^{10}$ $S*atm^{0.25}*K/cm$ and 275 kJ/mol in [36], $8.3*10^6$ $S*atm^{0.25}*K/cm$ and 198.4 kJ/mol in [35]). Once the parameters for the electronic conductivity were established, the polarization curves were simulated. A satisfactory agreement was found both at 600°C and 650°C. A moderate lack of agreement was observed at 29% H_2 in proximity of the OCV, a zone that is mostly affected by the leakage current effects. Overall, the results were satisfactory, and the estimated parameters were considered reliable. Therefore, the simulation results could be used to gain more insight in the cell behavior. Specifically, Figure 3a reports in the insert the predicted amount of the leakage current. The leakage current decreased at increasing the temperature and the total current extracted from the cell, while it increased upon increasing the concentration of the reactant. Its influence was more pronounced at the OCV, while it quickly dropped and almost vanished upon decreasing the voltage. Importantly, the

calculations show that the cell was highly inefficient in terms of current extraction, since the maximum leakage current reached up to 26% of the maximum total current extracted (70 mA/cm^2 vs. 264 mA/cm^2 at 650°C and 97% H_2). These results do confirm that an insulating barrier is required in case the cell has to be optimized to perform in applications.

4.2 CO electro-oxidation

The same approach followed in the case of the H_2 oxidation rates was applied for the oxidation rate of CO. Also in this case, the kinetic parameters (Tab. 5) and the reaction orders where estimated under the assumption that the charge transfer coefficients in the Butler-Volmer equation were equal to 0.5 and the number of exchanged electrons was 2. Panel d of Figure 5 shows the comparison between the polarization resistance measured in the EIS tests and the values calculated by the model. The best agreement was found by assuming an order equal to 1 for CO and to zero for CO_2. These orders reveal that the kinetics were determined by a charge transfer step involving a species associated to the non-dissociative adsorption of CO and that no inhibition was given by CO_2. This result is in line with the observations of Costa-Nunes et al. [12] over Cu-Ceria-YSZ anodes, who found a positive dependence of the CO oxidation rate upon increasing the CO pressure in CO/N_2 mixture. A positive first order dependence on CO was also reported by Setoguchi et al. [38] on Ni-SDC anodes, though at higher temperatures than the present ones.

The kinetic rate was the applied in the simulation of the polarization curves of the CO/CO_2 mixtures (Fig. 4). In this case, no parameters were fit, being also the electrolyte electronic conduction parameters already fixed. Good agreement was obtained under all the explored conditions, except for the simulations at 48.5% CO at

650°C and 68% CO at 600°C, where a lack of agreement was evident in the top part of the curve. The reason for this was related to the leakage current, which hindered too much the OCV: a good agreement was restored (dashed lines in Fig. 4) when the simulations were carried out by assuming a value of 1.8 S*atm$^{0.25}$*K/cm for the electronic conduction of the SDC electrolyte, almost a half of the one estimated for H_2 and used at higher CO concentration. This result is possibly in line with the fact that the electronic conductivity of SDC varies with the reduction potential, specifically it increases with a negative power on O_2 (Eq. 18):

$$\sigma_{Elect}^{Electronic} \propto \left(P_{O2}^{An}\right)^{-1/4} \propto \left(P_{CO}^{An}\right)^{+1/2} \qquad (34)$$

Considering the equilibrium of CO combustion, the relationship of Eq. (34) results in a positive dependence of the electronic conductivity on the partial pressure of CO: that is, a decrease of the conductivity was experimentally expected upon lowering the concentration of CO, which was not fully reproduced by the model. Indeed, SDC was also present in the porous matrix of the anode, and a dependence of the local pressure was not accounted for. This effect could also explain the moderate underestimation of the OCV zone in the simulations at 29% H_2 and 650°C (Fig. 3a), and in general the predicted variation of the OCV which was not observed in the experiments with H_2. Nonetheless, its entity in the case of H_2 tests is modest. Notwithstanding with these features, the simulations were satisfactory and the estimation of the parameters of the CO oxidation rate were considered reliable.

4.3 Experiments with syngas mixtures

Once the kinetic equations of the H_2 electro-oxidation, of the CO electro-oxidation and of the O_2 reduction were independently derived, the polarization

experiments with syngas mixtures could be simulated on a fully predictive basis, with no adjustment of any parameter. The results of this comparison is shown in the panels a and b of Figure 2: a close description was obtained under all the conditions of temperature and composition explored, both for the OCV values and for the evolution of the polarization curves. This result is significant, since it proves that a scheme considering the co-oxidation of CO and H_2 well fitted the data; however, it does not entirely prove the necessity for a co-oxidative scheme to achieve the best description. In principle, the data could be described based either on a scheme where the H_2 oxidation was active in the presence of WGS, with no intervention of the CO oxidation, or based on a scheme wherein only the CO oxidation was active with a contribution from the RWGS reaction. These possibilities were explored and the results are shown in Figure 7a and b, with respect to the experiments carried out at 600°C. In the simulations, the WGS reaction was considered as fast enough to be equilibrated and both the effects of the direct and the reverse rates were taken into consideration. A coherent value for the a_v ratio was introduced ($1.8*10^6$ m^2/m^3, consistent with a porosity of 40% and a particle diameter of 2 μm, according to Ref. [22]). In both cases, the schemes did not allow to closely simulate the experimental curves, and important lacks of agreement were observed in the description of the OCV values and of the concentration effect. Additionally, these results show that a switch from a regime governed by the oxidation of H_2 to a regime governed by the oxidation of CO (a condition often invoked when the pressure of CO is higher than that of H_2) could not satisfactorily describe the data. It is also worthy to note that the WGS/RWGS equilibrium never played a significant role, given that the effects related to the conversion of the reactants were modest.

Overall, the model analysis indicated that the parallel oxidation of CO and H_2 allowed to achieve the closest agreement with the data, much better than those

obtained with other schemes. This results supports the presence of a co-oxidative route in the reactive scheme of syngas combustion, which could be specific for the anodic formulation tested in the present IT-SOFC and likely associated to the properties of Ceria. The possibility of activating a co-oxidative route is promising, since it could allow to minimize the polarization losses, although it should be investigated under conditions where the cell microstructure is optimized and a wider experimental field can be explored. Nonetheless, the data discussed are kinetically informative and therefore capable of giving meaningful indications about the intrinsic chemical processes. A cell possibly closer to the application would be useful to point out the diffusive effects that higher conversion enhances due to the changes in the local gas composition.

5. Conclusions

The development of IT-SOFCs requires the experimental efforts to be accompanied by numerical tools, able to quantify the contributions of the different chemical, electrochemical and physical phenomena occurring in the cells. In this work, a one dimensional dynamic model of the cell was applied to rationalize the polarization behavior and the EIS results of SDC-electrolyte supported IT-SOFCs, tested over a wide range of experimental conditions, including syngas mixtures and biogas, between 600°C and 700°C. The cells had Cu/Pd/CZ80 composite anodes, prepared via infiltration of a porous SDC scaffold, and LSCF cathodes. The cells revealed active in the combustion of syngas at varying H_2 to CO ratio, and the activation of a co-oxidative route could be envisaged, wherein H_2 and CO were electro-oxidized in parallel. To gain a deeper insight in this behavior, a kinetic investigation was carried out. The kinetics of the H_2 oxidation and of the CO

oxidation were analyzed individually, based on polarization and EIS experiments with H_2/N_2 mixtures and CO/CO_2 mixtures at varying the partial pressure of the reactants. The model allowed to derive global, power-law type rate equations for the electro-oxidation of H_2, the electro-oxidation of CO and the reduction of O_2. Based on the kinetics extracted independently, the experiments with syngas mixtures were thus simulated on a fully predictive basis: a close description of the experimental data was obtained and the co-oxidation behavior could be rationalized.

From an experimental viewpoint, the parasitic leakage current always showed a significant impact, resulting in OCV values lower than the theoretical ones (0.9 V at 650°C and 0.95V at 600°C with humidified H_2 flow) and amounting to a consistent share of the total current extracted from the cell. Low OCV values were found also in the presence of biogas, which were associated to the limiting role of the dry-reforming activity of the anode catalyst.

Overall, the presence of a co-oxidative route opens up interesting possibilities for further optimization of the IT-SOFCs tested in this work. Required improvements include the adoption of adequate protective barriers in order to limit the parasitic current, and the optimization of the electrode microstructure to increase the cell performance.

Acknowledgements

Funding from MIUR-Italy (PRIN project 2010KHLKFC) is gratefully acknowledged.

References

[1] D.J.L. Brett, A. Atkinson, N.P. Brandon, S.J. Skinner, Chemical Society Reviews, 37 (2008) 1568.

[2] D.F. Yang, X.G. Zhang, S. Nikumb, C. Deces-Petit, R. Hui, R. Maric, D. Ghosh, Journal of Power Sources, 164 (2007) 182-188.

[3] X. Zhang, M. Robertson, C. Deces-Petit, W. Qu, O. Kesler, R. Maric, D. Ghosh, Journal of Power Sources, 164 (2007) 668-677.

[4] E.V. Tsipis, V.V. Kharton, Journal of Solid State Electrochemistry, 12 (2008) 1367-1391.

[5] S. McIntosh, R.J. Gorte, Chem. Rev., 104 (2004) 4845-4865.

[6] S. McIntosh, J.M. Vohs, R.J. Gorte, Electrochimica Acta, 47 (2002) 3815-3821.

[7] R.J. Gorte, S. Park, J.M. Vohs, C.H. Wang, Adv. Mater., 12 (2000) 1465-1469.

[8] Z.H. Bi, J.H. Zhu, Journal of Power Sources, 195 (2010) 3097-3104.

[9] S. McIntosh, J.M. Vohs, R.J. Gorte, Electrochem. Solid State Lett., 6 (2003) A240-A243.

[10] J. Hanna, W.Y. Lee, Y. Shi, A.F. Ghoniem, Prog. Energy Combust. Sci., 40 (2014) 74-111.

[11] A.M. Sukeshini, B. Habibzadeh, B.P. Becker, C.A. Stoltz, B.W. Eichhorn, G.S. Jackson, J. Electrochem. Soc., 153 (2006) A705-A715.

[12] O. Costa-Nunes, R.J. Gorte, J.M. Vohs, Journal of Power Sources, 141 (2005) 241-249.

[13] W.G. Bessler, J. Warnatz, D.G. Goodwin, Solid State Ion., 177 (2007) 3371-3383.

[14] D.G. Goodwin, H. Zhu, A.M. Colclasure, R.J. Kee, J. Electrochem. Soc., 156 (2009) B1004-B1021.

[15] J. Hanna, W.Y. Lee, A.F. Ghoniem, J. Electrochem. Soc., 160 (2013) F698-F708.

[16] V. Yurkiv, D. Starukhin, H.-R. Volpp, W.G. Bessler, J. Electrochem. Soc., 158 (2011) B5-B10.

[17] H.Y. Zhu, R.J. Kee, V.M. Janardhanan, O. Deutschmann, D.G. Goodwin, J. Electrochem. Soc., 152 (2005) A2427-A2440.

[18] A. Leonide, Y. Apel, E. Ivers-Tiffee, ECS Transactions, 19 (2009) 81-109.

[19] Y.X. Shi, N.S. Cai, C. Li, C. Bao, E. Croiset, J.Q. Qian, Q. Hu, S.R. Wang, J. Electrochem. Soc., 155 (2008) B270-B280.

[20] A. Bertei, J. Mertens, C. Nicolella, Electrochimica Acta, 146 (2014) 151-163.

[21] A. Bertei, B. Nucci, C. Nicolella, Chem. Eng. Sci., 101 (2013) 175-190.

[22] J. Deseure, Y. Bultel, L. Dessemond, E. Siebert, P. Ozil, J. Appl. Electrochem., 37 (2007) 129-136.

[23] J.M. Vohs, R.J. Gorte, Adv. Mater., 21 (2009) 943-956.

[24] A. Fuerte, R.X. Valenzuela, M.J. Escudero, L. Daza, International Journal of Hydrogen Energy, 39 (2014) 4060-4066.

[25] I. Riess, J. Electrochem. Soc., 128 (1981) 2077-2081.

[26] R.T. Leah, N.P. Brandon, P. Aguiar, Journal of Power Sources, 145 (2005) 336-352.

[27] M. Sahibzada, R.A. Rudkin, B.C.H. Steele, I.S. Metcalfe, J.A. Kilner, Evaluation of PEN structures incorporating supported thick film Ce0.9Gd0.1O1.95 electrolytes, Electrochemical Society Inc, Pennington, 1997.

[28] H.Y. Zhu, R.J. Kee, J. Electrochem. Soc., 153 (2006) A1765-A1772.

[29] S. Primdahl, M. Mogensen, J. Electrochem. Soc., 146 (1999) 2827-2833.

[30] H. Iwai, Y. Yamamoto, M. Saito, H. Yoshida, Energy, 36 (2011) 2225-2234.

[31] R. Krishna, J.A. Wesselingh, Chem. Eng. Sci., 52 (1997) 861-911.

[32] H.Y. Zhu, R.J. Kee, Journal of Power Sources, 117 (2003) 61-74.

[33] B.A. Finlayson, Introduction to Chemical Engineering Computing, John Wiley & Sons, Hoboken, New Jersey, 2012.

[34] S. Sameshima, N. Furukawa, Y. Hirata, T. Shimonosono, Ceramics International, 40 (2014) 6279-6284.

[35] S.L. Shen, Y.P. Yang, L.J. Guo, H.T. Liu, Journal of Power Sources, 256 (2014) 43-51.

[36] D. Cui, Q. Liu, F.L. Chen, Journal of Power Sources, 195 (2010) 4160-4167.

[37] M.R. Kosinski, R.T. Baker, Journal of Power Sources, 196 (2011) 2498-2512.

[38] T. Setoguchi, K. Okamoto, K. Eguchi, H. Arai, J. Electrochem. Soc., 139 (1992) 2875-2880.

Nomenclature

a_v = surface to volume ratio [m^2/m^3]

B = permeability coefficient according to the Kozeny-Carman relationship

C_{DL} = double layer capacity [F/m^2]

C_i = concentration of the ith species [mol/m^3]

C_{tot} = total concentration of the gas phase [mol/m^3]

$D_{i,j}^{Mol}$ = molecular binary diffusion of the ith species in the jth species [m^2/s]

D_i^{Knu} = Knudsen diffusion of the ith species [m^2/s]

E_0 = reference potential [V]

E_{Cell} = cell voltage [V]

E_{Act} = activation energy [J/mol]

E_m = mean cell voltage [V]

E_{Nernst} = Nernstian potential [V]

E_p = amplitude of the voltage perturbation [V]

F = Faraday constant [C/mol]

F^{In} = inlet molar flow rate [mol/s]

F^{Out} = outlet molar flow rate [mol/s]

i_m = mean current density [A/cm^2]

i_0 = exchange current density [A/cm^2]

$i_{O^{2-}}$ = ionic current density [A/cm^2]

i_p = amplitude of the current perturbation [A/cm^2]

i_{Tot} = total current density [A/cm^2]

$i_{e^-}^{leakage}$ = electronic leakage current density [A/cm^2]

J_i = molar flow of the ith species [mol/m^2/s]

j = imaginary unit

k = pre-exponential factors of the kinetic rate

L = layer thickness [m]

n_{e^-} = number of electrons exchanged in the electro-oxidation reaction

P = pressure [Pa]

P_i = partial pressure of the ith species [Pa]

R = gas constant [J/mol/K]

R_{Act} = activation polarization resistance [Ω*cm^2]

R_{Ohm} = ohmic resistance [Ω*cm^2]

r_j = rate of the jth reaction [mol/m^2/s]

T = temperature [K]

t = time [s]

t_P = two-period time interval [s]

x_i = molar fraction of the ith species

Z_{Diff} = diffusion impedance [$\Omega*cm^2$]

Z_{Global} = global impedance [$\Omega*cm^2$]

Z_{Total} = total impedance [$\Omega*cm^2$]

z = axial coordinate [m]

Greek Symbols

α = charge transfer coefficient

δ = Kronecker delta

ε = electrode porosity

η_{Act} = activation overpotential [V]

μ = dynamic viscosity of the gas mixture [Pa*s]

ν = stoichiometric coefficient

σ = conductivity [S/m]

τ = electrode tortuosity

φ = phase

ω = frequency [Hz]

Subscripts and superscripts

An = anodic

Cat = cathodic

Eff = effective

Elect = electrolyte

electro = referred to the electrochemical reaction

i = ith species

j = jth species

Ox = oxidation

Re = reduction

W = referred to the interface between the electrode and the electrolyte

Tables

Table 1: morphological properties of the cell.

Anode (Cu/Pd/CZ80/SDC)	
Thickness	150 μm
Porosity	0.4
Anode Diameter	2 cm
Particle Diameter	2 μm
Cathode (LSCF)	
Thickness	40 μm
Porosity	0.4
Cathode Diameter	1.1 cm
Particle Diameter	2 μm
Electrolyte (SDC)	
Thickness	380 μm

Table 2: model equations and boundary conditions.

Mass Balance	$$\varepsilon \cdot \frac{dC_i}{dt} = -\frac{dJ_i}{dz} + a_v \cdot \sum_j^{Nreactions} \nu_{ij} \cdot r_j$$	(1)
Dusty Gas Model	$$\frac{dC_i}{dz} = -\sum_{j \neq i}^{Nspecie} \frac{C_j \cdot J_i - C_i \cdot J_j}{C_{tot} \cdot D_{i,j}^{Mol,Eff}} - \frac{J_i}{D_i^{Knu,Eff}} - \frac{B}{\mu} \cdot \frac{C_i}{D_i^{Knu,Eff}} \cdot \frac{dP}{dz}$$	(2)
Ideal Gas Law	$$P \cdot x_i = C_i \cdot RT$$	(3)
Cell Potential	$$E_{Cell} = E_{Nernst} - R_{Ohm} \cdot i_{O^{2-}} - \eta_{Act}^{An} - \eta_{Act}^{Cat}$$	(4)
Anode Activation	$$i_{O^{2-}} = i_0^{An} \cdot \left[\exp\left(\frac{\alpha_A^{An} \cdot n_{e^-} \cdot F \cdot \eta_{Act}^{An}}{RT} \right) - \exp\left(-\frac{\alpha_C^{An} \cdot n_{e^-} \cdot F \cdot \eta_{Act}^{An}}{RT} \right) \right]$$	(5)
Cathode Activation	$$i_{O^{2-}} = i_0^{Cat} \cdot \left[\exp\left(\frac{\alpha_A^{Cat} \cdot n_{e^-} \cdot F \cdot \eta_{Act}^{Cat}}{RT} \right) - \exp\left(-\frac{\alpha_C^{Cat} \cdot n_{e^-} \cdot F \cdot \eta_{Act}^{Cat}}{RT} \right) \right]$$	(6)
Nernst Potential	$$E_{Nernst} = E_0 - \frac{RT}{n_{e^-} \cdot F} \cdot \ln \prod_i^{Nspecie} \left(P_i^W \right)^{\nu_i^{electro}}$$	(7)
Current Balance	$$i_{Tot} = i_{O^{2-}} - i_{e^-}^{leakage}$$	(8)
Leakage Current	$$i_{e^-}^{leakage} = \left(\frac{P^\theta}{\exp\left(-\frac{4RT}{F \cdot \left(-\frac{RT}{4F} \ln P_{O_2}^W + \eta_{Act}^{Cat} \right)} \right)} \right)^{1/4} \cdot i_{O^{2-}} \cdot \frac{\exp\left(\frac{F \cdot E_{cell}}{RT} - 1 \right)}{1 - \exp\left(-\frac{F \cdot i_{O^{2-}}}{RT} \cdot \frac{L_{Elect}}{\sigma_{Elect}^{ionic}} \right)}$$	(9)
Boundary Conditions		
Gas/Electrode Interface (z = 0)		
Anode Side	$$\mathrm{F}_{\mathrm{An}}^{\mathrm{In}} \cdot x_i^0 - \mathrm{F}_{\mathrm{An}}^{\mathrm{Out}} \cdot x_i^{Out} - J_i\big\vert_{z=0}$$	(10)
Cathode Side	$$\mathrm{F}_{\mathrm{Cat}}^{\mathrm{In}} \cdot x_i^0 - \mathrm{F}_{\mathrm{Cat}}^{\mathrm{Out}} \cdot x_i^{Out} - J_i\big\vert_{z=0}$$	(11)
Pressure	$$P = P_0$$	(12)
Electrode/Electrolyte Interface (z = L)		
Molar Flow	$$J_{z=L} = \nu_i^{electro} \cdot \frac{i_{O^{2-}}}{n_{e^-} \cdot F}$$	(13)

Table 3: kinetic equations and material properties.

H_2 oxidation exchange current density	$i_{0,H_2}^{An} = k_{H_2}^{Ox} \cdot T \cdot \exp\left(-\frac{E_{Act}^{OxH_2}}{RT}\right) \cdot P_{H_2}^{0.47}$	(14)
CO oxidation exchange current density	$i_{0,CO}^{An} = k_{CO}^{Ox} \cdot T \cdot \exp\left(-\frac{E_{Act}^{OxCO}}{RT}\right) \cdot P_{CO}$	(15)
O_2 reduction exchange current density	$i_0^{Ca} = k_{O_2}^{\mathrm{Re}} \cdot T \cdot \exp\left(-\frac{E_{Act}^{\mathrm{Re}}}{RT}\right) \cdot P_{O_2}^{0.33}$	(16)
Ionic Conductivity	$\sigma_{Elect}^{Ionic} = \frac{\sigma_{Elect}^{Ionic,0}}{T} \cdot \exp\left(-\frac{E_{Act}^{Ionic}}{RT}\right)$	(17)
Electronic Conductivity	$\sigma_{Elect}^{Electronic} = \frac{\sigma_{Elect}^{Electronic,0}}{T} \cdot \exp\left(-\frac{E_{Act}^{Electronic}}{RT}\right) \cdot \left(P_{O_2}^{W}\right)^{-1/4}$	(18)

Table 4: equations of the impedance problem.

Current Input	$i_{Tot}(t) = i_m + i_p \cdot \sin(\omega \cdot t)$	(19)
Voltage Output	$E_{Cell}(t) = E_m + E_p \cdot \sin(\omega \cdot t + \varphi)$	(20)
Impedance	$Z = \frac{E_p}{i_p} \cdot (\cos(\varphi) + j \cdot \sin(\varphi))$	(21)
Anodic Polarization	$\left(R_{Act}^{An}\right)^{-1} = \frac{i_0^{An} n_{e^-} F}{RT} \cdot \left[\alpha_A^{An} \exp\left(\frac{\alpha_A^{An} \cdot n_{e^-} \cdot F \cdot \eta_{Act}^{An}}{RT}\right) + \alpha_C^{An} \exp\left(-\frac{\alpha_C^{An} \cdot n_{e^-} \cdot F \cdot \eta_{Act}^{An}}{RT}\right)\right]$	(22)
Cathode Polarization	$\left(R_{Act}^{Cat}\right)^{-1} = \frac{i_0^{Cat} n_{e^-} F}{RT} \cdot \left[\alpha_A^{Cat} \exp\left(\frac{\alpha_A^{Cat} \cdot n_{e^-} \cdot F \cdot \eta_{Act}^{Cat}}{RT}\right) + \alpha_C^{Cat} \exp\left(-\frac{\alpha_C^{Cat} \cdot n_{e^-} \cdot F \cdot \eta_{Act}^{Cat}}{RT}\right)\right]$	(23)
Diffusion Impedance	$Z_{Diff} = Z - R_{Ohm} - R_{Act}^{An} - R_{Act}^{Cat}$	(24)
Total Impedance	$Z_{Total} = Z_{Diff} + R_{Ohm} + \frac{R_{Act}^{An}}{1 + j \cdot \omega \cdot R_{Act}^{An} \cdot C_{DL}^{An}} + \frac{R_{Act}^{Cat}}{1 + j \cdot \omega \cdot R_{Act}^{Cat} \cdot C_{DL}^{Cat}}$	(25)

Table 5: Kinetic and material parameters.

Anode	
$k_{H_2}^{Ox}$	0.47 A/cm^2/K/atm$^{0.47}$
$E_{Act}^{OxH_2}$	73 kJ/mol
k_{CO}^{Ox}	34.2 A/cm^2/K/atm
E_{Act}^{OxCO}	108 kJ/mol
Cathode	
$k_{O_2}^{\mathrm{Re}}$	8.7*10^3 A/cm^2/K/atm$^{0.33}$
E_{Act}^{Re}	139 kJ/mol
Electrolyte	
$\sigma_{Elect}^{Ionic,0}$	1.39*10^4 S*K/cm
E_{Act}^{Ionic}	48.5 kJ/mol
$\sigma_{Elect}^{Electronic,0}$	3.5*10^8 S*atm$^{0.25}$*K/cm
$E_{Act}^{Electronic}$	220 kJ/mol

Table 6: OCV, maximum extracted current (at 0.5 V) and corresponding H_2 conversion for the polarization experiments with humidified H_2/N_2 mixtures.

T [°C]	**x H_2**	**OCV [V]**	**i [mA/cm^2]**	**χ H_2 %**
600	97%	0.948	182.1	3.9
	68%	0.950	178.4	5.3
	48.5%	0.948	161.4	6.9
650	97%	0.902	241.8	4.7
	68%	0.904	227.3	6.4
	48.5%	0.909	213.2	8.4
	29%	0.907	197.4	13.0

Table 7: OCV, maximum extracted current (at 0.5 V) and corresponding CO conversion for the polarization experiments with humidified CO/CO_2 mixtures.

T [°C]	x CO	OCV [V]	i [mA/cm^2]	χ CO %
600	94%	0.953	152.0	3.1
	70%	0.944	128.9	3.5
650	94%	0.913	228.9	4.6
	70%	0.905	190.5	5.2
	48.5%	0.899	166.0	6.5

Figures

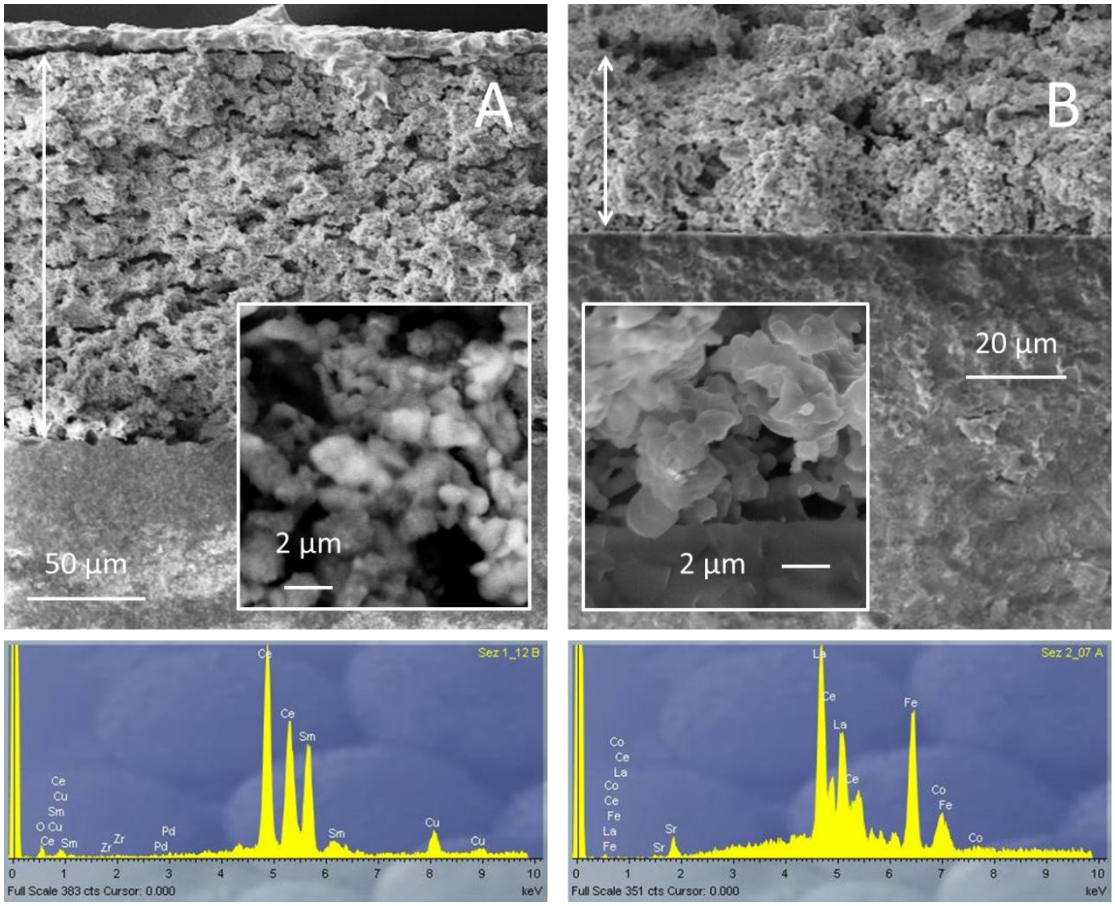

Figure 1

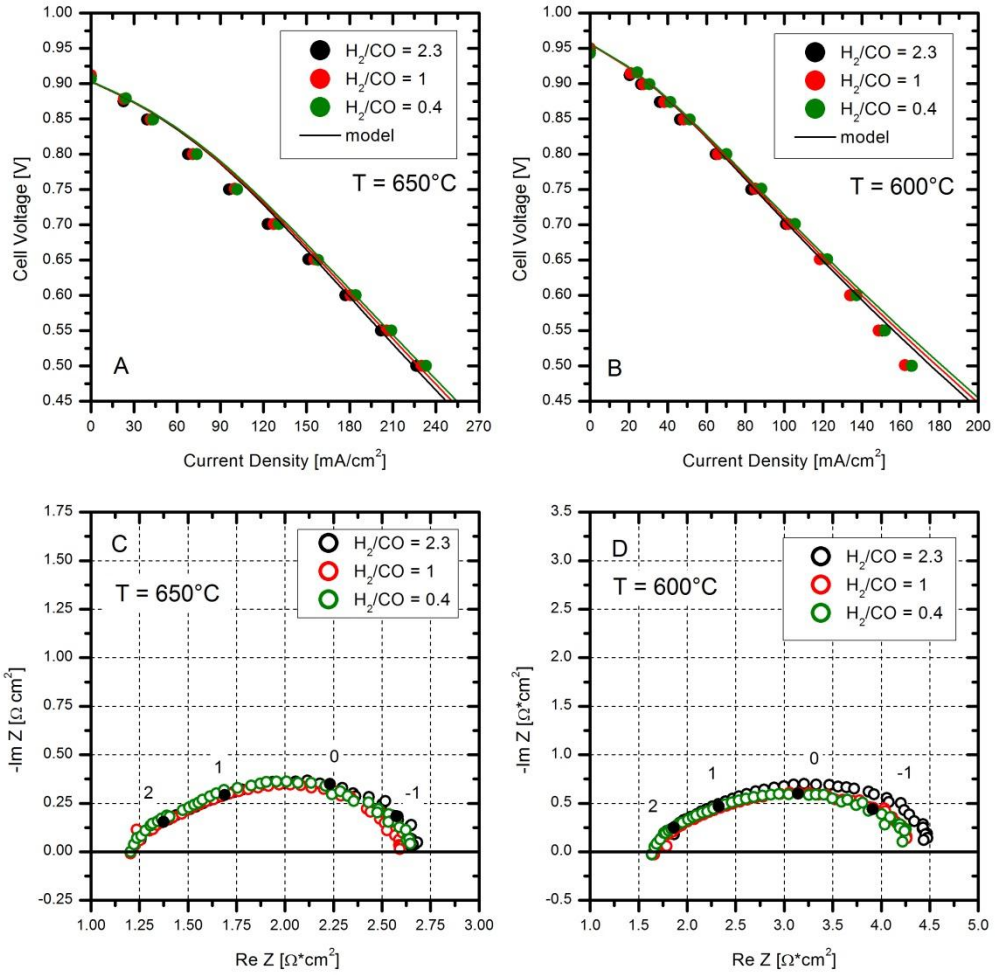
A
B
C
D
T = 650°C
T = 600°C
H2/CO = 2.3
H2/CO = 1
H2/CO = 0.4
model
Cell Voltage [V]
Current Density [mA/cm2]
-Im Z [Ω cm2]
-Im Z [Ω*cm2]
Re Z [Ω*cm2]
0
1
2
-1

Figure 2

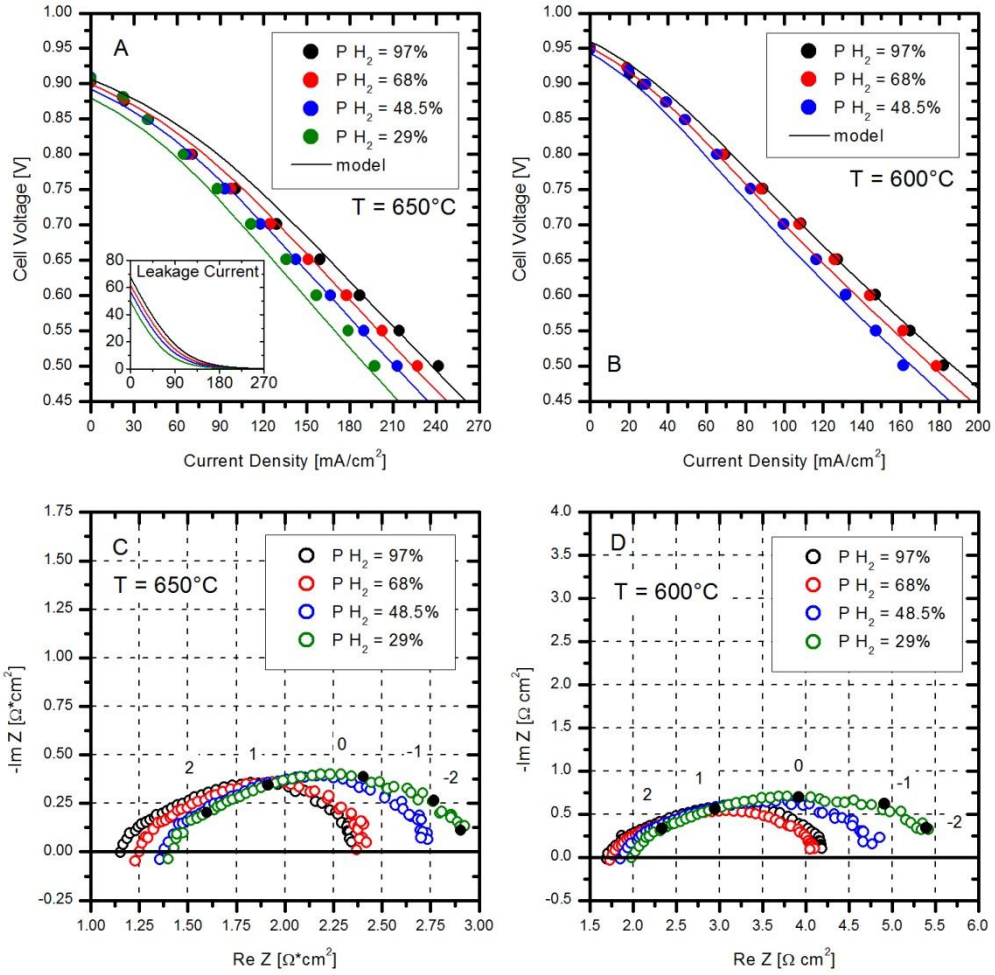

Figure 3

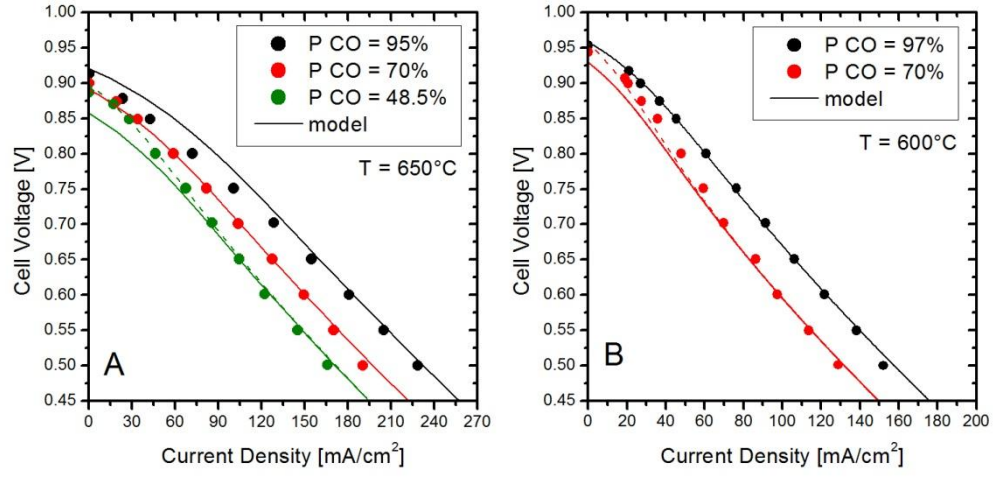

Figure 4

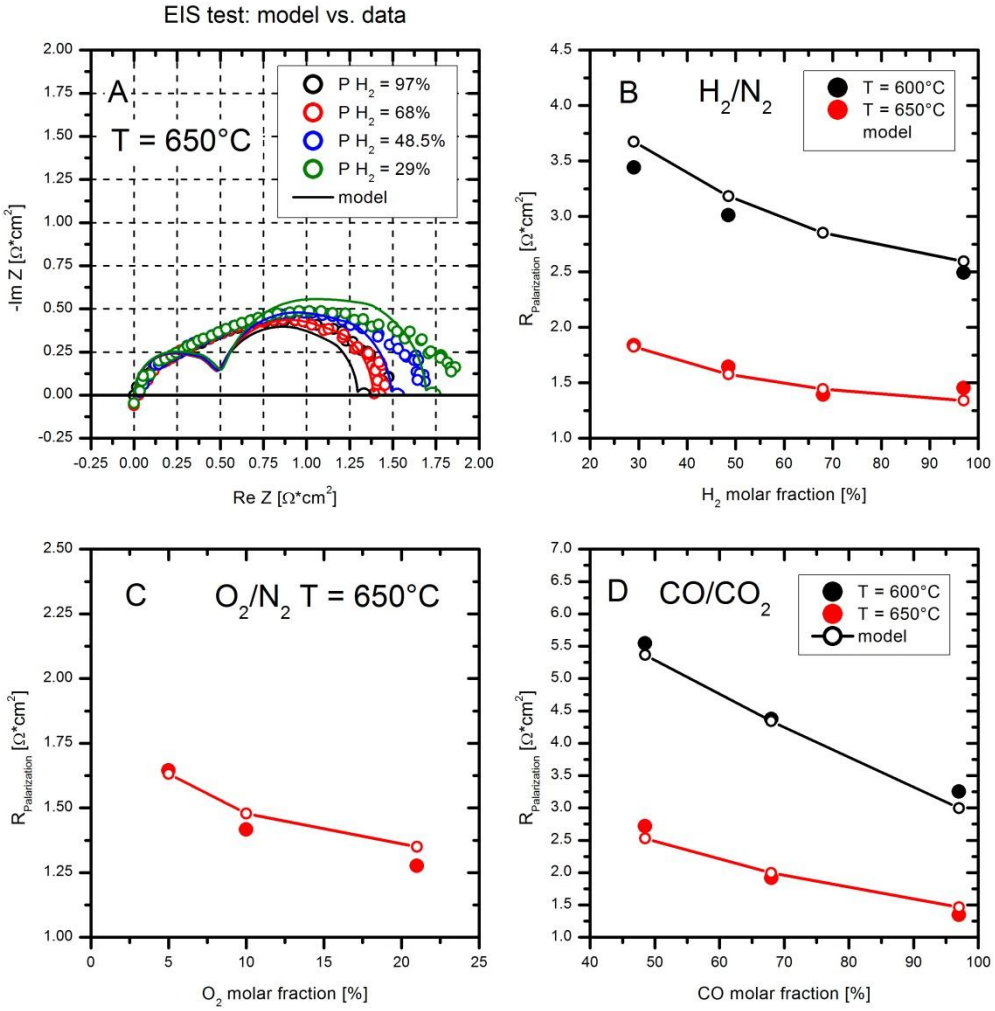

Figure 5

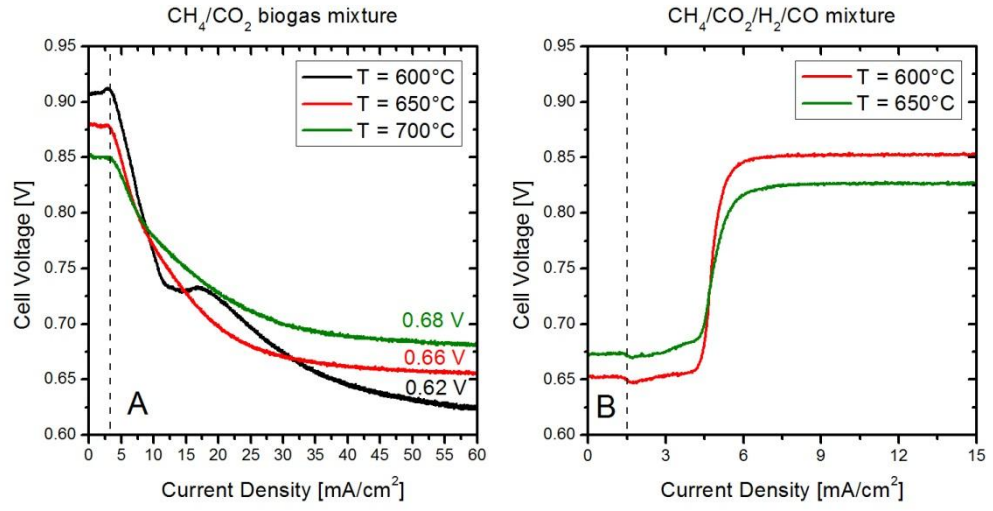

Figure 6

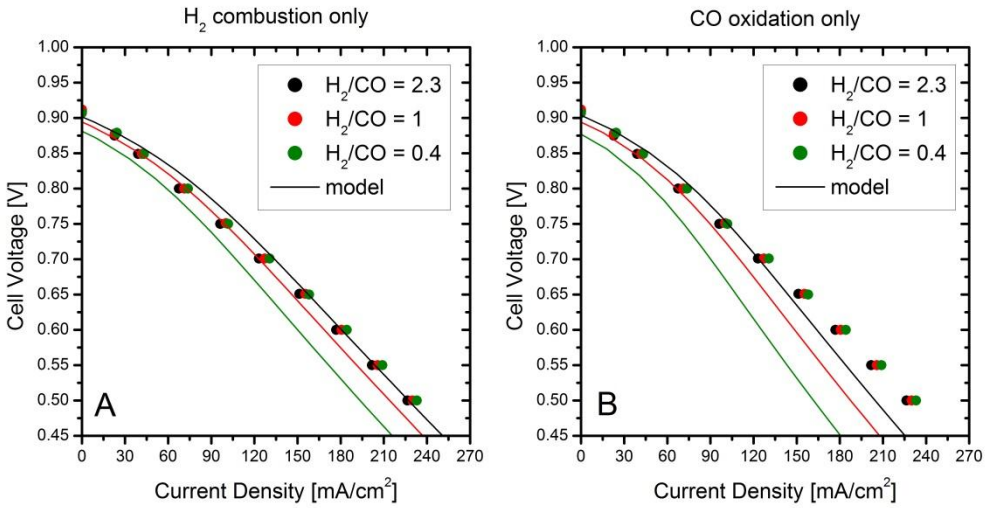
H2 combustion only
CO oxidation only
Cell Voltage [V]
Current Density [mA/cm2]
H2/CO = 2.3
H2/CO = 1
H2/CO = 0.4
model
A
B

Figure 7

Figure Captions

Figure 1 – SEM pictures of the anode (A) and of the cathode (B).

Figure 2 – Experiments with syngas mixtures. A) polarization curve at 650°C. B) polarization curve at 600°C. C) EIS spectra at 650°C. D) EIS spectra at 600°C. Lines are model simulations, symbols are data. (●) H_2 = 68%, CO = 29%; (●) H_2 = 48.5%, CO = 48.5%; (●) H_2 = 29%, CO = 68%. Constant 3% H_2O humidification.

Figure 3 – Experiments with H_2/N_2 mixtures. A) polarization curve at 650°C. B) polarization curve at 600°C. C) EIS spectra at 650°C. D) EIS spectra at 600°C. Lines are model simulations, symbols are data. (●) H_2 = 97%; (●) H_2 = 68%, N_2 = 29%; (●) H_2 = 48.5%, N_2 = 48.5%; (●) H_2 = 29%, N2 = 68%. Constant 3% H_2O humidification.

Figure 4 – Experiments with CO/CO_2 mixtures. A) polarization curve at 650°C. B) polarization curve at 600°C. Lines are model simulations, symbols are data. (●) CO = 94%, CO_2 = 3%; (●) CO = 70%, CO_2 = 27%; (●) CO = 48.5%, CO_2 = 48.5%. Constant 3% H_2O humidification. Dashed lines are simulations performed with $\sigma_{Elect}^{Electronic,0}$ = 1.8 S*atm$^{0.25}$*K/cm

Figure 5 – Panel A) Comparison between the experimental and the simulated EIS spectra for the H_2/N_2 experiment at 650°C. B) Comparison between the experimental and simulated R_{Pol} for the H_2/N_2 experiment at 600°C (●) and 650°C

(●). C) Comparison between the experimental and simulated R_{Pol} for the O/N_2 experiment at 650°C (●). D) Comparison between the experimental and simulated R_{Pol} for the CO/CO_2 experiment at 600°C (●) and 650°C (●).

Figure 6 – OCV variation as a function of time during the experiments with biogas and CH_4-rich mixtures at increasing temperature. Panel A) CH_4 = 75%, CO_2 = 25%, dry basis. B) CH_4 = 50%, CO_2 = 20%, H_2 = 20%, CO = 10%, dry basis.

Figure 7 – Simulation of the polarization curves collected at 650°C. Panel A) only H_2 oxidation is considered. B) only CO oxidation is considered.